Visible and near-infrared characterization and modeling of nanosized holographic-polymer-dispersed liquid crystal gratings

Francesco Vita, Antigone Marino, Volodymyr Tkachenko, and Giancarlo Abbate
INFM Coherentia and Dipartimento di Scienze Fisiche, Università di Napoli "Federico II," Via Cinthia, Monte S. Angelo, 80126 Naples, Italy

Daniele E. Lucchetta, Luigi Criante, and Francesco Simoni
INFM and Dipartimento di Fisica e Ingegneria dei Materiali e del Territorio, Università Politecnica delle Marche, Via Brecce Bianche, 60131 Ancona, Italy

(Received 19 January 2005; published 11 July 2005)

We have studied the electro-optical and angular behavior of holographic-polymer-dispersed liquid crystal gratings at different wavelengths, in the visible and in the near-infrared range. As usual in these kinds of materials, a strong polarization dependent behavior was observed. Our samples showed very high diffraction efficiency for *p*-polarized radiation at 1.55 μm, which is very interesting for many possible applications in the telecom field. However, we also observed a very unusual behavior for visible *p*-polarized light and we try to suggest some explanation for that. By analyzing the angular dependence of the diffraction efficiency, we could measure the components of the permittivity modulation tensor and infer important information about the main parameters involved in the grating structure: the degree of phase separation and the anisotropy in the liquid crystal droplet distribution. In our opinion, this simple and nondestructive methodology can be very useful for studying these kinds of materials and getting information on their morphology, in view of optimizing their properties. Finally, we discuss the role of the refractive index optical dispersion in order to describe the behavior of these materials at different wavelengths. These remarks are especially important when properties in the infrared range are extrapolated from measurements in the visible.

DOI: 10.1103/PhysRevE.72.011702 PACS number(s): 61.30.Pq, 42.40.Pa, 42.70.Df, 42.25.Fx

I. INTRODUCTION

The utility of Diffraction Bragg gratings (DBGs) is well known in a large number of optical applications [1]. Holography is an effective and simple technique to produce Bragg gratings characterized by high diffraction efficiency (DE) and low losses. In particular, switchable and/or tunable DBG can be the basic element of many photonics devices (lasers, switches, filters, multiplexers, cross connectors), to be used in optical communication systems [2].

These functionalities can be obtained by exploiting the peculiar properties of liquid crystals (LCs). Widely used in the display technology, LCs have a number of features (high birefringence, high electro-optic coefficient, transparency, good integration in silicon devices, low cost) that make them very attractive for any kind of photonic application, also in the telecom field [3]. In past years a new kind of electrically switchable holographic grating has been recorded in LC-polymer composite materials [4–6]. These gratings, usually known as H-PDLC (holographic-polymer-dispersed liquid crystals), are produced by curing, under a laser interference pattern, an isotropic photosensitive liquid mixture, containing basically a prepolymeric material, a liquid crystal, and a photoinitiator. The result of the recording process is a grating consisting of a periodic distribution of small LC droplets, embedded in a polymeric matrix: larger droplets and a higher LC concentration are found in correspondence of the dark fringes, whereas smaller LC domains and polymer rich stripes are obtained in correspondence of the bright fringes. Because of the difference in refractive index between the polymer and the LC, the spatial modulation of the LC content produces a modulation in the average refractive index. The resulting optical phase grating can be easily switched off by applying an external voltage: LC molecules arrange themselves parallel to the electric field and, if the materials are properly chosen, a good index matching between droplets and polymer matrix can be obtained.

H-PDLC gratings can be proposed as active elements for a number of photonic DBG based devices for telecom applications [7]. Of course, in order to match the requirements of optical communication systems, these materials should be optimized to work at the telecom wavelengths, typically in the near IR (NIR) range: in this spectral region, gratings should show high diffraction efficiency, angular selectivity, low losses, low driving voltages, and fast switching times. All these properties are directly connected to the main structural features of the material, i.e., degree of phase separation, LC alignment inside the droplets, droplet size, shape, and orientation. On the other hand, these morphological parameters are dependent on the variables involved in the fabrication process: the physical and chemical properties of each single component, their concentration in the initial mixture, the curing parameters (light intensity, exposure time, sample temperature), and the sample geometry (grating spacing and thickness).

In recent years a great effort has been made to achieve a deeper understanding of the H-PDLC microscopic structure [6]. Different techniques have been used: nuclear magnetic resonance (NMR) [8,9], scanning electron microscopy (SEM) [10,11], atomic force microscopy (AFM) [11], dy-

namic light scattering (DLS) [9,12], and optical and electro-optical characterizations [13–17].

In this work we present an electro-optical characterization of H-PDLC gratings, both in the visible and in the NIR region. In order to analyze our experimental data, we propose a simple effective model that takes into account the main structural features of the sample, such as the degree of phase separation and anisotropic alignment of the LC, as well as the dispersive behavior of all the involved materials (polymer and liquid crystal). By using this approach we can obtain some quantitative indication about the sample morphology and, at the same time, make reliable extrapolations on the behavior of the grating optical properties at different wavelengths. This information can be subsequently used to optimize the grating design, leading to the realization of new optical devices and prototypes. In fact, until now few studies have been performed on LC composite materials at telecom wavelengths [17–22]. Moreover, the extension to the NIR range of experimental data obtained in the visible requires particular care. Our study can give some important indication in this direction.

II. MATERIALS AND EXPERIMENT

We have studied a few samples of H-PDLC transmission gratings realized in the laboratories of the Università Politecnica delle Marche, in the frame of an Italian National Research Project [23]. They were made starting from a solution of the monomer dipentaerythrol-hydroxyl-penta-acrylate DPHPA (39.8% in weight), the cross-linking stabilizer monomer N-vinylpyrrolidinone (20% in weight), the liquid crystal E7 by Merck (40% in weight) and a mixture of the photoinitiator Rose Bengal and the coinitiator N-phenylglycine (0.2% in weight). The chemical structures of these components are reported elsewhere [4].

The cells containing the samples were prepared using indium-tin-oxide (ITO) coated glasses, separated by Mylar spacers (thickness 23 μm), and were filled by capillarity at a fixed temperature of 65 °C. The photosensitive mixture was cured by the interference pattern of two coherent *s*-polarized Ar-ion laser beams ($\lambda = 0.514$ μm). The interference angle was chosen to get a grating spacing $\Lambda = 1.72$ μm and fringes orthogonal to the cell glasses. The exposure time was fixed at 10 min and the laser intensity at 357 mW/cm^2 per beam, with a spot diameter of 6 mm. In the LC rich regions we expect droplets with average size in the range 100–200 nm, according to previous SEM analyses performed by us in samples of the same mixture. This is also consistent with a morphological investigation that we performed on similar samples with a lower content of LCs finding sizes in the range 50–130 nm [24] and with observations of other authors [10].

At $\lambda = 0.589$ μm and at room temperature (20 °C), the material refractive indices are, for the polymer, $n_p = 1.526$ and, for the liquid crystal, $n_o = 1.521$ and $n_e = 1.746$. With these optical parameters, an applied electric field of suitable amplitude should completely switch off the grating. In fact, a suitable strong electric field will reorient the droplet LC director along the normal to the cell substrates. In this situation, an impinging light at quasinormal incidence experiences a refractive index close to the ordinary one of the LC, independently of the light polarization direction, hence the H-PDLC appears as an optically homogeneous material.

In the following, we define the diffraction efficiency as the ratio between the diffracted beam intensity and the sum of the transmitted and diffracted light intensities. In this way we ignore all the effects related to the losses for reflection, scattering, and absorption, the latter being very small for visible light but becoming more important in the NIR, due to the presence of the ITO in our substrates. In most cases, as expected, our gratings operate in a typical Bragg diffraction regime, with just one diffracted beam and a negligible amount of light diffracted in higher orders. Some anomalous behavior will be discussed later on.

We performed measurements at four wavelengths: 0.532 μm (Nd:YAG laser second harmonic), 0.633 μm (He-Ne laser), 1.064 μm (Nd:YAG laser), and 1.55 μm (DFB laser diode). The sample temperature was held constant at 25.0± 0.1 °C via a suitable computer controlled hot stage. The external incidence angle was regulated by a motorized rotational stage, with an accuracy of 0.01°. The electro-optical properties were checked by applying an ac square voltage at a sufficiently high frequency, say 1 kHz, as usually made in order to avoid unwanted dc screening and current effects. The studied samples showed a very similar and reproducible behavior. However, the experimental data reported in the next sections all refer to the same sample.

III. EXPERIMENTAL RESULTS

We measured the angular response of our gratings at different wavelengths and for both polarizations. As expected, DE curves are peaked in correspondence of the wavelength dependent Bragg angle, according to the well-known formula

$$\sin \theta_B = \frac{\lambda}{2 n_0 \Lambda}, \tag{1}$$

with θ_B being the Bragg angle, λ the incident light wavelength, and n_0 the average refractive index of the medium in which the angle is measured. Experimental values for the Bragg angles correspond to a grating pitch $\Lambda = 1.61$ μm. This is slightly smaller than the spacing of the recording interference pattern, probably due to a shrinkage effect during the curing process. A small slant ($\sim 0.3°$) in the grating fringes was also revealed by comparing the angular positions of positive and negative diffraction orders.

Dotted lines in Figs. 1(a)–1(d)[1] show the experimental data obtained for *s*-polarization: we observed high DE in the visible ($\sim 90\%$), much lower in the NIR (10–30%). The electro-optical response of the sample is shown in Fig. 2: at 0.633 μm, DE is reduced to one-half at 11 V/μm and vanishes at 14 V/μm; at 1.55 μm, a small initial DE decreasing is obtained at weak fields, from 1 to 2 V/μm, after that DE stabilizes not going to zero, indicating that a perfect index matching of the two components is never reached.

The results for *p*-polarization are shown in Figs. 1(e) and 1(f). In this case the observed behavior is quite different: we

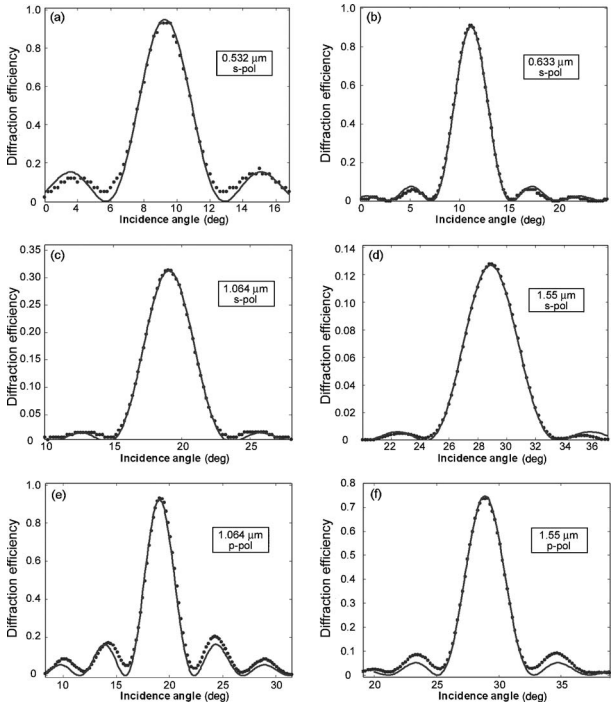

FIG. 1. Diffraction efficiency dependence on the incidence angle for different wavelengths and polarizations: experimental data (dots) and theoretical fits (lines).

got very good efficiency in the NIR (70–90%), whereas in the visible we did not observe the expected DE peak around the Bragg angle. However, by applying an electric field the angular behavior of the DE was continuously changing (Fig. 3): at 7.8 V/μm, we got a curve very similar to the one obtained for *s*-polarization with no field; a further increase of the electric field led to the switching off of the grating, as expected.

Ordinary PDLC materials, cured under uniform light exposure, do not show such a polarization dependent behavior because the droplet directors are randomly oriented in the bulk of the sample. On the contrary, a higher efficiency in *p*-polarization is typical for most transmission H-PDLC made of similar mixtures [6,17]. This is in contrast with the

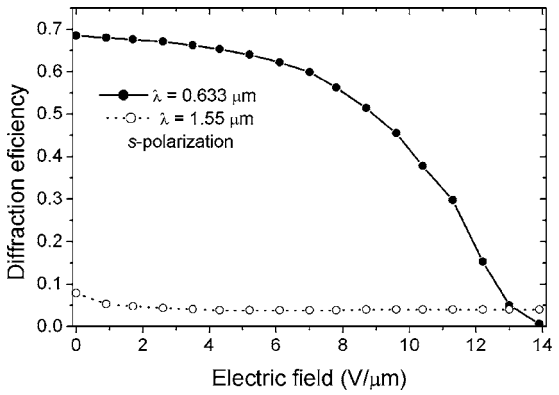

FIG. 2. Diffraction efficiency vs applied electric field for *s*-polarized light at two different wavelengths: 0.633 μm (closed circles) and 1.55 μm (open circles).

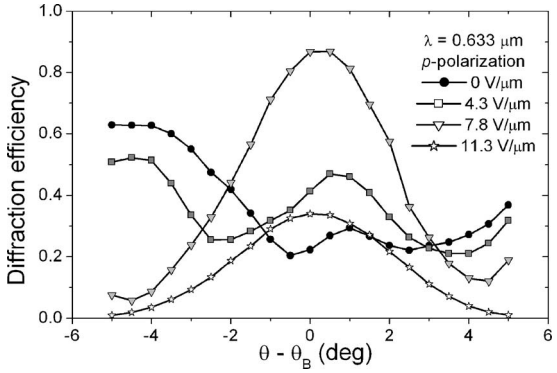

FIG. 3. Diffraction efficiency vs incidence angle for different applied electric fields, *p*-polarization and $\lambda = 0.633$ μm.

properties of isotropic gratings, which should show a higher coupling constant, i.e., a higher DE, for *s*-polarized light. This is a clear indication of the anisotropic nature of the H-PDLC gratings, due to a preferred orientation of the LC domains, in this case along the grating vector.

We point out some differences that our results show as compared with others reported in literature on similar H-PDLC gratings. For instance, in Ref. [17] the switching field value is much lower than the one observed in our experiment. Since the switching field is related to the droplet size, we expect a smaller droplet dimension in our case. In addition, a surfactant was added in the sample of Ref. [17] that can explain that lower value, even for a comparable droplet size. Furthermore, we notice that, at zero field, for *s*-polarized visible light, the observed DE is much higher than the one observed for *p*-polarization in the same wavelength range [compare Fig. 1(b) with Fig. 3]. This is in contrast to what was reported in [17] and to our measurements in the NIR [see Figs. 1(c)–1(f)]. We shall discuss this point in detail in Sec. V A.

IV. THEORY

Different theories can be used to study holographic gratings [1,25]. Two-coupled-wave Kogelnik theory [26] is widely used to describe thick, isotropic gratings. However, an extension of the theory to optically anisotropic materials (Montemezzani and Zgonik [27]) is needed when dealing with samples showing a polarization dependent behavior [13,14,16,17,28–30]. The main assumptions and final results are here summarized for the general anisotropic case.

In a coordinate system with the x axis normal to the fringes, assumed orthogonal to the containing glasses, and the z axis normal to the sample (Fig. 4), a lossless transmission grating is described by a dielectric tensor in the following form:

$$\vec{\vec{\varepsilon}}(x) = \vec{\vec{\varepsilon}}^{0} + \vec{\vec{\varepsilon}}^{1} \cos\frac{2\pi x}{\Lambda}, \tag{2}$$

with $\vec{\vec{\varepsilon}}^{0}$ and $\vec{\vec{\varepsilon}}^{1}$ representing the average value and the amplitude of modulation of the permittivity tensor, respectively. At any wavelength and incidence angle, the diffraction efficiency $\eta_{s/p}$ is ruled by the expression

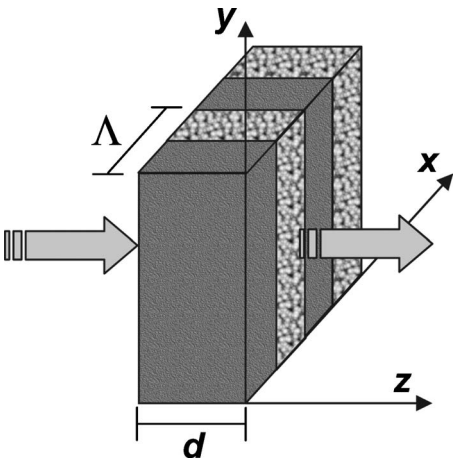

FIG. 4. Sample geometry and reference system. Λ is the grating pitch and d the sample thickness.

$$\eta_{s/p} = \frac{\sin^2\sqrt{\nu^2+\xi^2}}{1+\xi^2/\nu^2}, \tag{3}$$

where the subscripts denote the two light polarizations. The quantities ν and ξ, usually referred as grating strength and detuning parameter, are defined as follows:

$$\nu = \frac{\pi d(\hat{e}_1 \cdot \vec{\varepsilon}^{\,1} \cdot \hat{e}_2)_{s/p}}{2\lambda\sqrt{n_1^0 n_2^0}\cos\theta_1\cos\theta_2\cos\delta_1\cos\delta_2}, \tag{4}$$

$$\xi = \frac{\pi d}{\lambda}(n_1^0\cos\varphi_1 - n_2^0\cos\varphi_2). \tag{5}$$

In these expressions, d is the grating thickness, δ is the walk-off angle between the energy propagation (Poynting vector) direction and the wave-vector direction, θ is the angle (inside the sample) between the energy propagation vector and the sample normal, φ is the angle (inside the sample) between the wave vector and the sample normal, n^0 is the average refractive index, $\hat{e}$ is the beam polarization unit vector, and the subscripts 1 and 2 refer to the zeroth and first order diffracted beam, respectively. Actually, for the materials considered here, the walk-off angle δ is very small and can be neglected. By the same token, the implicit dependence of n^0 on the incidence angle plays a minor role in the calculations. In fact, we performed check calculations without assuming these approximations, but we did not get any significant difference.

When the Bragg condition [Eq. (1)] is fulfilled, a complete symmetry between the zeroth and the first diffracted beam is observed ($\varphi_1 = \varphi_2$); as a consequence the detuning parameter is zero and DE reaches its maximum value [Eq. (3)].

Assuming a diagonal form for the permittivity tensor (no coupling between p and s polarization was experienced during experimental measurements) the coupling constant $\hat{e}_1 \cdot \vec{\varepsilon}^{\,1} \cdot \hat{e}_2$ results to be

$$(\hat{e}_1 \cdot \vec{\varepsilon}^{\,1} \cdot \hat{e}_2)_s = \varepsilon_{yy}^1, \tag{6a}$$

$$(\hat{e}_1 \cdot \vec{\varepsilon}^{\,1} \cdot \hat{e}_2)_p = \varepsilon_{xx}^1\cos\theta_1\cos\theta_2 - \varepsilon_{zz}^1\sin\theta_1\sin\theta_2, \tag{6b}$$

for s and p polarization, respectively, with ε_{ii}^1 indicating the diagonal elements of the modulation tensor.

V. MODELING AND DISCUSSION

A. Angular response data fitting

As a first step in our analysis, we fitted our experimental angular curves with the theoretical expression in Eq. (3). The components of the permittivity modulation tensor and the thickness were chosen as fitting parameters, for each curve. According to Eqs. (6a) and (6b), we were sensitive to ε_{yy}^1 when probing in s polarization, and to ε_{xx}^1 in p polarization. In the latter case, instead of introducing a third variable in the fit, we preferred to assume the material as uniaxial, with the optical axis parallel to the grating vector, i.e., $\varepsilon_{zz}^1 = \varepsilon_{yy}^1$. This assumption is commonly found in literature [13,20,29,30] and is connected to the symmetry of the LC droplets in the direction orthogonal to fringes.

The fitting curves are shown as continuous lines in Figs. 1(a)–1(f): the agreement with the experimental data is very good in s polarization and less in p polarization. In this case, the model is not able to fit exactly the side lobes (compare with similar fits in [20,22,31]). Releasing the assumption on the uniaxiality of $\vec{\varepsilon}^{\,1}$ does not improve the fit. In fact, the main discrepancy is that DE does not reach zero in the minima between the central and the side peaks. This is probably due to an attenuation of the permittivity modulation through the depth of the sample (tapering of the refractive

TABLE I. Results of the fits on the angular DE curves. For the two NIR wavelengths the second value of the thickness d is obtained from p-polarized light measurements.

λ (μm)	d(μm)	$\varepsilon_{yy\text{-}zz}^1$	ε_{xx}^1
0.532	33.4±0.3	0.0279±0.0005	
0.633	33.1±0.2	0.0235±0.0003	
1.064	32.2±0.1	0.0188±0.0001	0.0558±0.0009
	36.5±0.3		
1.55	33.0±0.3	0.0159±0.0001	0.0475±0.0005
	36.9±0.4		

index profile) [32]. The best fit parameters are reported in Table I for the different wavelengths: the order of magnitude is in agreement with published data [13,29]; moreover, ε^1_{xx} is always larger than $\varepsilon^1_{yy/zz}$, indicating a preferred alignment of the LC molecules in the direction of the optical grating. This is commonly observed in H-PDLC transmission samples containing E7 liquid crystal [6,17]. Both components of the permittivity modulation tensor are clearly decreasing with the wavelength, due to the refractive index dispersion of the involved materials. Finally, the thickness values obtained by the *s*-polarization fits are reasonably higher than the spacer thickness as expected, and in good agreement with each other. The ones obtained by *p*-polarization fits are slightly different: this could be connected with the lower accuracy of the fit, trying to compensate the mismatch in the side lobes by increasing the thickness.

As evident from Eqs. (3) and (4), for a given permittivity modulation tensor, DE can be moved from a maximum to a minimum by changing the sample thickness. Thus the previously mentioned discrepancy in the polarization behavior of the DE between our measurements and those reported in [17] should be analyzed in this frame. From our measurements of $\vec{\vec{\varepsilon}}^1$ we can compute DE at the Bragg angle ($\xi=0$) for different values of d: for instance, a 8 μm sample yields $\eta_s=0.09$ and $\eta_p=0.49$, whereas a 13 μm sample gives $\eta_s=0.22$ and $\eta_p=0.90$. These values are compatible to the ones reported in [17]. It follows that increasing d, up to a given value corresponding to $\nu=\pi/2$, produces an increase of η for both polarizations. In our sample, however, the value of thickness is so high that we get a maximum DE for *s*-polarization, while we enter overmodulation ($\nu>\pi/2$) and loose the Bragg regime for *p*-polarization. We shall come back on the latter point in Sec. V C. The wavelength effect in the NIR range pushes farther the thickness corresponding to the overmodulation limit, so that it is not reached in our sample.

In conclusion, even if DE is definitely the most important grating feature from an application point of view, it is convenient to refer to the permittivity modulation when comparing different samples and evaluating their properties.

B. Morphological model

As a second step, we tried to connect the obtained values for the permittivity modulation tensor with the material optical constants and the grating structure. Actually, a lot of factors should be taken into account to describe the microscopic structure of a HPDLC sample: the shape, dimension, and orientation of the LC droplets (and the correspondent dispersion), as well as the alignment of the LC director inside each droplet (and the order parameter) [33]. Most of these morphological details are unknown or highly dependent on the mixture composition, geometrical parameters, and on curing process details. Necessarily this approach would be either extremely complex (and involving a high number of fitting parameters) or based on quite drastic assumptions.

We propose a model in which:

(1) α is the fraction of liquid crystal molecules not phase separated and randomly trapped in the polymer network; they concur with the polymer to form the matrix in which the LC droplets are embedded and cannot reorient under an applied electric field;

(2) β is a phenomenological parameter taking into account the effect of the fraction of liquid crystal phase separated and preferentially oriented in a given direction, namely the x direction according to the experimental indications; and

(3) finally, the remaining amount of the LC molecules is assumed to be phase separated and (on average) isotropically oriented.

Thus α and β can be viewed as an effective optical contrast and an anisotropy parameter, respectively. This approach will reduce the number of fitting parameters, while maintaining a reasonable description of the dependence of the optical behavior on the sample morphology.

In this simplified description, the ith diagonal component of the average (anisotropic) permittivity tensor $\vec{\vec{\varepsilon}}^0$, and the corresponding average refractive index tensor $\vec{\vec{\varepsilon}}^0$, are easily calculated to be

$$\varepsilon_i^0 = (n_i^0)^2 = f_P\varepsilon_P + \beta f_{LC}\varepsilon_{LC,i} + (1-\beta)f_{LC}\varepsilon_{iso}, \tag{7}$$

where f_P and f_{LC} are, respectively, the fraction of polymer (monomer+cross-linker) and liquid crystal in the initial mixture, $\varepsilon_P=(n_P)^2$ is the polymer permittivity, $\varepsilon_{iso}=\frac{1}{3}(n_e^2+2n_o^2)$ is the LC isotropic permittivity, and $\varepsilon_{LC,i}$ represents the ith diagonal component of the LC permittivity tensor.

We can also calculate the (isotropic) permittivity ε_{mat} of the polymer matrix as

$$\varepsilon_{mat} = \frac{f_P}{f_P + f_{LC}\alpha}\varepsilon_P + \frac{f_{LC}\alpha}{f_P + f_{LC}\alpha}\varepsilon_{iso}. \tag{8}$$

According to this picture, the grating structure is generated by the optical contrast between the stripes of homogeneous polymer/LC matrix and the stripes containing the LC droplets. We assume the two kinds of layers to have the same thickness (this was confirmed in [10] for similar materials) and model the permittivity modulation profile according to Eq. (2). (The real modulation profile could not be exactly sinusoidal. In that case, in order to use coupled-wave theory, we should apply a Fourier expansion to our profile. This would add a coefficient in front of $\vec{\vec{\varepsilon}}^1$. However, for our sample this coefficient is quite close to 1, due to our recording geometry.)

In this case the ith component of the permittivity modulation tensor $\vec{\vec{\varepsilon}}^1$ is simply the difference between the average permittivity and the polymer matrix one:

$$\varepsilon_i^1 = \varepsilon_i^0 - \varepsilon_{mat}. \tag{9}$$

In Fig. 5, we report the values for the components of the permittivity modulation tensor, as resulted by the angular fits, and the relative fitting curves calculated with our model. Again, *s* polarization gives better results than *p* polarization, but points in *p* polarization are affected by a larger error due to the poorer accuracy in the angular fits. The values of α and β that better fit our experimental values for the permittivity modulation tensor are $\alpha=0.44\pm0.01$ and $\beta=0.138\pm0.008$.

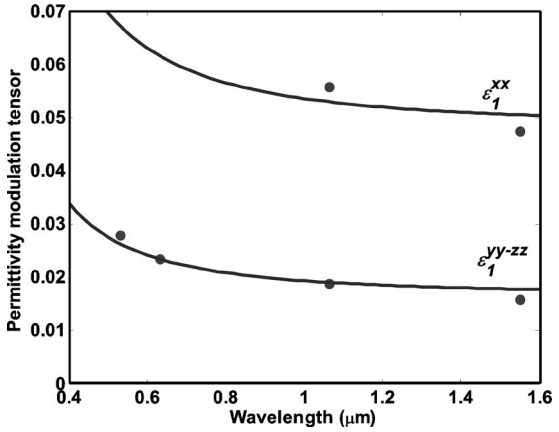

FIG. 5. Components of the permittivity modulation tensor vs wavelength: dots correspond to the values reported in Table I; continuous lines are the best fit curves on these points, according to the model described in the text.

A comparison of these data to other ones reported in literature requires some care, due to different definitions used by different authors, so that at this stage it can be only qualitative. Moreover, it is generally accepted, as we mentioned above, that the grating morphology strongly depends on many parameters that can vary from experiment to experiment. For instance, our value of α implies that the polymer matrix contains 23% of LC, a result in good agreement with the value measured in [28] (19.4%). In a similar way we can calculate the quantity $\beta/(1-\alpha)$, i.e., the ratio between the effective fraction of aligned LC and the total amount of phase separated LC. The value obtained (0.25) can be compared to the LC order parameter reported in [14] ($\sim$0.3), which is a different way to indicate a similar characteristic.

C. Comments on the effects of the electric field

In the experimental section, we showed the anomalous behavior observed with *p*-polarized visible light (Fig. 3). From the upper curve reported in Fig. 5, we could extrapolate the value of $\varepsilon^1_{yy/zz}$ at visible wavelengths: it is quite high and results in a grating overmodulation, i.e., in $\nu > \pi/2$. In this condition a drastic change in DE angular dependence is expected because a decrease of the Bragg peak in favor of the side maxima is observed for increasing $\nu > \pi/2$ (at $\nu = \pi$, Bragg peak amplitude gets a null value and a minimum is obtained). However, in our case it was not possible to fit the experimental angular dependence of the DE with the coupled-wave model, even considering overmodulation.

Although different reasons can be involved in producing the observed phenomenon, a critical one should be connected with the actual diffraction regime of our gratings. A detailed discussion on the limits of the Bragg and Raman-Nath regimes is found in [1]: as a matter of fact, the diffraction regime depends not only on the value of the Q factor, defined as

$$Q = \frac{2\pi\lambda d}{n_0\Lambda^2}\frac{1}{\cos\theta}, \tag{10}$$

but on the relative values of the Q and ν parameters. In particular, Bragg and Raman-Nath regimes are, respectively, defined by the inequalities:

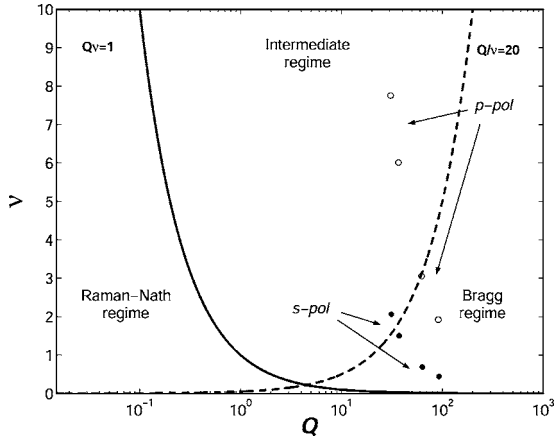

FIG. 6. Diffraction regime diagram as a function of the grating strength ν and the thickness parameter Q, according to Eqs. (11). Closed and open circles represent gratings studied with *s*-polarized and *p*-polarized light, respectively, at four wavelengths (0.532, 0.633, 1.064, and 1.55 μm). For each polarization, wavelength is decreasing with ν (the shorter the wavelength, the higher the respective circle position in the diagram).

$$Q/2\nu > 10, \tag{11a}$$

$$Q\nu < 1. \tag{11b}$$

These inequalities define three areas in the Q-ν plane, corresponding to three different diffraction conditions: the Bragg, the Raman-Nath, and an intermediate regime. For the last case, no analytical theory exists and a numerical approach has to be used.

Our grating positions in the Q-ν plane are shown in Fig. 6 for the different polarizations and wavelengths: for *s* polarization, our samples are always in the Bragg regime or very close to it (at $\lambda = 0.532$ μm); for *p* polarization points fall in the Bragg area for the longest wavelengths, but are in the intermediate area for the visible wavelengths, due to the high value of ν. This was confirmed observing an increase in the intensity of the higher order diffracted beams.

This consideration also provides a qualitative explanation to the observed behavior under an external voltage. The applied electric field induces the reorientation of the LC molecules along the z axis, resulting in a smaller value of the coupling constant $\hat{e}_1 \cdot \vec{\varepsilon}^1 \cdot \hat{e}_2$ and, hence, of ν. As a consequence, increasing the voltage, the points in the graph move down vertically and finally enter the Bragg regime area for a certain value of ν.

D. Comments on the effects of the optical dispersion

In all the previous expressions, there is always an implicit dependence on the wavelength through the refractive indices. We always allowed for the effects of dispersion in our calculations, assuming for all materials a Cauchy dispersion formula:

$$n = a + b/\lambda^2. \tag{12}$$

The Cauchy parameters used for pure polymer and liquid crystal are reported in Table II, the corresponding dispersion

TABLE II. Cauchy coefficients used to describe the dispersion curves for the polymer and the liquid crystal refractive indices.

Material	a	b (μm^2)
Polymer	1.5081	0.0061
LC, ordinary	1.4950	0.0090
LC, extraordinary	1.6858	0.0210

curves are plotted in Fig. 7. We point out that, while for the polymer the curve is the result of a direct spectroscopic measurement, for the LC we fitted few data reported in literature [34].

Optical dispersion has to be taken into account for at least two reasons. The first one is evident from Fig. 2: to completely switch off the grating, index matching has to be obtained at the working wavelength. In our case, due to the dispersion, this condition is better satisfied at 0.633 μm than at 1.55 μm (Fig. 7).

The second reason is even more important. When considering the grating in its on state, a major role in determining the permittivity modulation is played by the LC extraordinary refractive index. This index usually shows a much steeper decrease with increasing wavelength than the polymer one. When the material dispersion curves are not exactly parallel, a change in the wavelength, even producing a small variation in the absolute value of the refractive indices, may actually produce a relatively large variation in the index modulation, and thus in the observed diffraction efficiency.

This effect can be neglected in gratings recorded in a single material, where the modulation tensor $\vec{\varepsilon}^1$ is only slightly affected by changing the wavelength range. However, the role of dispersion is very important to predict in a reliable way the behavior of gratings recorded in composite materials, e.g., H-PDLC. This is especially true when the efficiency in the infrared range is extrapolated from measurements in the visible range. An example of the importance of this effect is shown in Fig. 8, where two curves showing DE vs wavelength are plotted: the first one is obtained neglecting dispersion, assuming for the permittivity modulation tensor the value measured at 0.633 μm, while the second one is computed using the dispersion coefficients reported in Table II. The disagreement is evident and, in general, is more pronounced for thicker samples. Quite obviously, the experimental points are much better fitted by the second curve. Correspondingly, the first curve gives more and more unreliable predictions the further we move from the wavelength region where the refractive indices were measured.

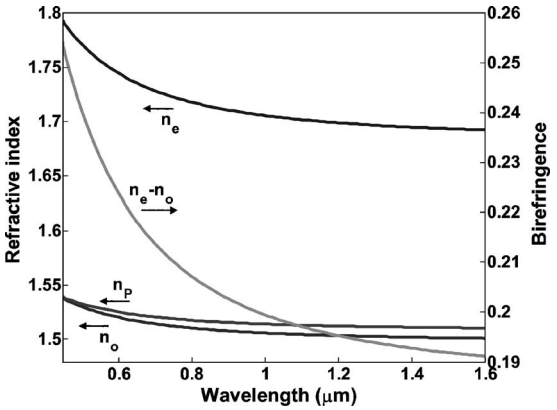

FIG. 7. Dispersion curves used in modeling H-PDLC samples.

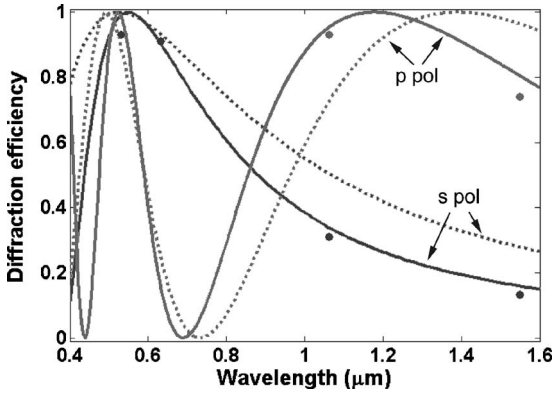

FIG. 8. Experimental DE values (points) and two different theoretical curves: including optical dispersion (continuous line), and neglecting it (dotted line).

VI. CONCLUSIONS

We used an approach based on the analysis of the angular dependence of the diffraction efficiency at different wavelengths to get information on two effective parameters involved in the H-PDLC structure: the degree of phase separation and the anisotropy in the LC distribution. Even if very simplified, our model makes possible an easy and nondestructive comparison between different samples and different fabrication procedures. In this way, we may be able to get a higher control on the grating structure and, hence, on the overall performances. However, a direct analysis by scanning electron microscopy and a deeper investigation of the microscopic dynamics of the curing process would be important to complement and confirm our findings.

Finally, an additional but necessary step, in order to design optimized devices for photonic applications, is complete knowledge of the optical parameters of all the used materials and their dispersion curves at the operation wavelengths. It is also evident that a proper material choice, generally different from those made in the visible range, is necessary to get the best performances in the NIR range.

ACKNOWLEDGMENT

D.E.L., L.C., and F.S. acknowledge support from EU project MICROHOLAS, Contract No. STRP 511437.

[1] T. K. Gaylord and M. G. Moharam, Proc. IEEE **73**, 894 (1985).
[2] L. Eldada, Rev. Sci. Instrum. **75**, 575 (2004).
[3] W. A. Crossland, T. V. Clapp, T. D. Wilkinson, I. G. Manolis, A. G. Georgiou, and B. Robertson, Mol. Cryst. Liq. Cryst. Sci. Technol., Sect. A **413**, 2499 (2004).
[4] R. L. Sutherland, L. V. Natarajan, V. P. Tondiglia, and T. J. Bunning, Chem. Mater. **1993**, 1533 (1993).
[5] R. L. Sutherland, V. P. Tondiglia, L. V. Natarajan, T. J. Bunning, and W. W. Adams, Appl. Phys. Lett. **64**, 1074 (1994).
[6] T. J. Bunning, L. V. Natarajan, V. P. Tondiglia, and R. L. Sutherland, Annu. Rev. Mater. Sci. **30**, 83 (2000).
[7] L. V. Natarajan, R. L. Sutherland, T. J. Bunning, and V. P. Tondiglia, Proc. SPIE **3292**, 44 (1998).
[8] G. S. Iannacchione, D. Finotello, L. V. Natarajan, R. L. Sutherland, V. P. Tondiglia, T. J. Bunning, and W. W. Adams, Europhys. Lett. **36**, 425 (1996).
[9] M. Vilfan, B. Zalar, A. K. Fontecchio, M. Vilfan, M. J. Escuti, G. P. Crawford, and S. Zumer, Phys. Rev. E **66**, 021710 (2002).
[10] R. T. Pogue, L. V. Natarajan, S. A. Siwecki, V. P. Tondiglia, R. L. Sutherland, and T. J. Bunning, Polymer **41**, 733 (2000).
[11] M. De Sarkar, N. L. Gill, J. B. Whitehead, and G. P. Crawford, Macromolecules **36**, 630 (2003).
[12] I. Drevensek-Olenik, M. Jazbinsek, M. Sousa, A. K. Fontecchio, G. P. Crawford, and M. Copic, Phys. Rev. E **69**, 051703 (2004).
[13] M. Jazbinsek, I. Drevensek-Olenik, M. Zgonik, A. K. Fontecchio, and G. P. Crawford, J. Appl. Phys. **90**, 3831 (2001).
[14] M. E. Holmes and M. S. Malcuit, Phys. Rev. E **65**, 066603 (2002).
[15] A. Marino, F. Vita, V. Tkachenko, R. Caputo, C. Umeton, A. Veltri, and G. Abbate, Eur. Phys. J. E **15**, 47 (2004).
[16] R. L. Sutherland, J. Opt. Soc. Am. B **19**, 2995 (2002).
[17] R. L. Sutherland, L. V. Natarajan, V. P. Tondiglia, S. Chandra, C. K. Shepherd, D. M. Brandelik, S. A. Siwecki, and T. J. Bunning, J. Opt. Soc. Am. B **19**, 3004 (2002).
[18] G. Abbate, A. Marino, and F. Vita, Mol. Cryst. Liq. Cryst. Sci. Technol., Sect. A **398**, 269 (2003).
[19] P. Nagtegaele and T. V. Galstian, Synth. Met. **127**, 85 (2002).
[20] S. Harbour, T. Galstian, R. S. Akopyan, and A. V. Galstyan, Opt. Commun. **238**, 261 (2004).
[21] L. McKenna, L. S. Miller, and I. R. Peterson, Polymer **45**, 6977 (2004).
[22] A. D'Alessandro, R. Asquini, C. Gizzi, R. Caputo, C. Umeton, A. Veltri, and A. V. Sukhov, Opt. Lett. **29**, 1405 (2004).
[23] Research Project of National Interest (PRIN 2000) by Italian Ministry of Education and Research, *Devices for Routing In Optical Networks Using New Liquid Crystals Materials and Composites*.
[24] D. E. Lucchetta, A. Manni, R. Karapinar, L. Gobbi, and F. Simoni, Mol. Cryst. Liq. Cryst. Sci. Technol., Sect. A **375**, 397 (2002).
[25] M. Neviere and E. Popov, J. Imaging Sci. Technol. **41**, 315 (1997).
[26] H. Kogelnik, Bell Syst. Tech. J. **48**, 2909 (1969).
[27] G. Montemezzani and M. Zgonik, Phys. Rev. E **55**, 1035 (1997).
[28] J. J. Butler, M. S. Malcuit, and M. A. Rodriguez, J. Opt. Soc. Am. B **19**, 183 (2002).
[29] D. E. Lucchetta, L. Criante, and F. Simoni, J. Appl. Phys. **93**, 9669 (2003).
[30] D. E. Lucchetta, L. Criante, and F. Simoni, Opt. Lett. **28**, 725 (2003).
[31] C. Neipp, A. Beléndez, S. Gallego, M. Ortuño, I. Pascual, and J. T. Sheridan, Opt. Express **11**, 1835 (2003).
[32] H. Kogelnik, Bell Syst. Tech. J. **55**, 109 (1976).
[33] F. Simoni, *Nonlinear Optical Properties of Liquid Crystals and Polymer Dispersed Liquid Crystals* (World Scientific, Singapore, 1997).
[34] Merck datasheet; X. Wang, D. Wilson, R. Muller, P. Maker, and D. Psaltis, Appl. Opt. **39**, 6545 (2000); S. Brugioni and R. Meucci, J. Opt. A, Pure Appl. Opt. **6**, 6 (2004).